SYNTHESIS OF ZnO NANOMATERIALS, WO_x NANOPARTICLES AND WO_x/ZnO NANOCOMPOSITES FOR INHIBITION OF BACTERIAL GROWTH AND ORGANIC DYES REMOVAL

YING YUET LEE

UNIVERSITI SAINS MALAYSIA

2018

SYNTHESIS OF ZnO NANOMATERIALS, WO_x NANOPARTICLES AND WO_x/ZnO NANOCOMPOSITES FOR INHIBITION OF BACTERIAL GROWTH AND ORGANIC DYES REMOVAL

by

YING YUET LEE

Thesis submitted in fulfillment of the
requirements for the degree of
Master of Science

December 2018

ACKNOWLEDGEMENT

First and foremost, I would like to express my deepest gratitude to School of Materials and Mineral Resources Engineering, Universiti Sains Malaysia for giving me the opportunity to complete my research for MSc and for providing an appropriate and healthy environment as well as well-equipped with facilities for me to do my research work.

Many thanks must go to my project supervisor, Assoc. Prof. Ir. Dr. Pung Swee Yong for his invaluable advice and guidance throughout the course of this project. I could not have completed this work without his invaluable encouragement and support. I also give my appreciation to my co-supervisor Dr Ong Ming Thong from INFORMM for his endless help regarding all issues related to microbiological. Furthermore, special thanks to Dr. Pung Yuh Fen at University of Nottingham, Malaysia campus for letting me to visit her research group and valuable comments related to antibacterial susceptibility assay of this project.

Support staffs and technicians never receive enough thanks, but without them most of the research works would fall apart. Their assistance in utilization of equipment and recommendation in problem-solving are highly appreciated. I would greatly appreciate my postgraduate friends, who have helped and supported me in completion of my research for MSc.

Last but not least, I appreciate the financial support from research funding under FRGS (203/PBAHAN/6071327) for my MSc study.

TABLE OF CONTENTS

		Page
ACKNOWLEDGEMENT		**ii**
TABLE OF CONTENTS		**iii**
LIST OF TABLES		**vii**
LIST OF FIGURES		**ix**
LIST OF ABBREVIATIONS		**xivi**
LIST OF SYMBOLS		**xviii**
ABSTRAK		**xix**
ABSTRACT		**xx**
CHAPTER ONE: INTRODUCTION		
1.1	Research background	1
1.2	Problem statement	6
1.3	Research objectives and scopes of work	8
1.4	Dissertation outline	10
CHAPTER TWO: LITERATURE REVIEW		
2.1	Introduction	11
2.2	Water pollution in Malaysia	11
	2.2.1 Bacterial	13
	2.2.2 Organic dyes	15
2.3	AOP	16
	2.3.1 General semiconductor photocatalysis mechanism	18
	2.3.2 Other factors that contributing to the inactivation of bacteria	22
	2.3.3 Strategies to improve photocatalytic efficiency of semiconductor photocatalysts	29
2.4	Types of semiconductor photocatalysts	31
	2.4.1 ZnO	31
	2.4.2 WO_x	34
	2.4.3 Semiconductor nanocomposites	35

2.5 Synthesis of ZnO nanoparticles and WO_x nanoparticles 36

2.6 Antibacterial susceptibility assay 40

2.6.1 Dilution method 41

2.6.1(a) Broth dilution method 41

2.6.1(b) Agar dilution method 42

2.7 Photocatalytic study of organic dye removal by ZnO based particles 46

CHAPTER THREE: MATERIALS AND METHODOLOGY

3.1 Introduction 51

3.2 Raw materials and chemicals 53

3.3 Synthesis of semiconductor nanocomposites 54

3.3.1 Synthesis of ZnO submicron rods (MRs) 54

3.3.2 Synthesis of ZnO nanodisks (NDs) 55

3.3.3 Synthesis of WO_x nanoparticles (NPs) 55

3.3.4 Synthesis of WO_x/ZnO nanocomposites (NCs) 56

3.3.4(a) Effect of sodium tungstate dihydrate concentration 61

3.4 Characterization techniques 61

3.4.1 X-ray diffraction (XRD) 61

3.4.2 Field Emission Scanning Electron Microscopy (FESEM) and Energy Dispersive X-ray Spectroscopy (EDX) 62

3.4.3 Transmission Electron Microscopy (TEM), High-Resolution Transmission Electron Microscopy (HRTEM) and Selected Area Electron Diffraction (SAED) 62

3.4.4 Brunauer–Emmett–Teller (BET) 63

3.4.5 Fourier Transform Infrared Spectroscopy (FTIR) 63

3.4.6 Room Temperature Photoluminescence (RTPL) 63

3.4.7 Ultraviolet-Visible Spectroscopy (UV-Vis) 64

3.5 Photocatalytic degradation of organic dye using semiconductor photocatalysts 64

3.6 Antibacterial study using semiconductor nanoparticles 66

3.6.1 Preparation of test solution 66

3.6.2 Antibacterial susceptibility assay 66
3.6.3 Minimal Inhibitory Concentration (MIC) and Minimal Bactericidal Concentration (MBC) determinations 67

CHAPTER FOUR: RESULTS AND DISCUSSION

4.1 Introduction 70
4.2 Synthesis and characterization of ZnO MRs and ZnO NDs 70
4.2.1 Structural and optical properties 70
4.2.2 Growth mechanism of ZnO MRs and ZnO flower 81
4.2.3 Growth mechanism of ZnO NDs 83
4.2.4 Photocatalytic activity of ZnO MRs and ZnO NDs in RhB dye removal 85
4.2.5 Photocatalytic mechanism of ZnO particles in RhB dye removal 96
4.2.6 Antibacterial susceptibility assay 97
4.2.7 Antibacterial mechanism of ZnO MRs and ZnO NDs 103
4.3 Synthesis and characterization of WO_x NPs 106
4.3.1 Structural and optical properties 106
4.3.2 Growth mechanism of WO_x NPs 113
4.3.3 Photocatalytic activity of WO_x NPs in RhB dye removal 114
4.3.4 Photocatalytic mechanism of WO_x NPs in RhB dye removal 119
4.3.5 Antibacterial susceptibility assay 121
4.3.6 Antibacterial mechanism of WO_x NPs 124
4.4 Synthesis and characterization of WO_x/ZnO NCs 126
4.4.1 Structural and optical properties 126
4.4.2 Growth mechanism of WO_x/ZnO NCs 137
4.4.3 Photocatalytic activity of WO_x/ZnO NCs in RhB dye RhB dye removal 137
4.4.3(a) Photocatalytic activity of WO_x/ZnO NCs in BCG dye removal 145
4.4.4 Photocatalytic mechanism of WO_x/ZnO NCs in RhB dye removal 147
4.4.5 Antibacterial susceptibility assay 149

4.4.6 Antibacterial mechanism of WO_x/ZnO NCs 155
4.5 Summary 156

CHAPTER FIVE: CONCLUSIONS AND FUTURE WORKS

5.1 Conclusions 162
5.2 Future works 163

REFERENCES 164

APPENDICES

LIST OF PUBLICATIONS

LIST OF TABLES

		Page
Table 1.1	A comparison between ZnO and TiO_2 properties (Wei et al., 2015, Gorospe and Herrera, 2017)	5
Table 2.1	Antibacterial performance of ZnO-based semiconductor photocatalysts (GP: Gram-positive bacteria and GN: Gram-negative bacteria)	48
Table 2.2	Photodegradation of organic dyes using ZnO based nanocomposites.	50
Table 3.1	Precursors used for the synthesis of semiconductor nanoparticles	53
Table 3.2	Precursors used in the photocatalytic study for RhB and BCG dye removal	53
Table 3.3	Precursors and bacteria used in Minimal Inhibitory Concentration (MIC) and Minimal Bactericidal Concentration (MBC) assay	54
Table 3.4	Synthesis parameters for WO_x/ZnO nanocomposites	61
Table 4.1	The Minimal Inhibitory Concentration (MIC) of ZnO MRs and ZnO NDs against Gram-positive and Gram-negative bacteria (sample size, n = 3)	99
Table 4.2	The Minimal Bactericidal Concentration (MBC) of ZnO MRs and ZnO NDs against Gram-positive and Gram-negative bacteria (sample size, n = 3)	99
Table 4.3	The Minimal Inhibitory Concentration (MIC) and Minimal Bactericidal Concentration (MBC) of WO_x NPs against Gram-positive and Gram-negative bacteria	122
Table 4.4	Specific surface area of the samples	134
Table 4.5	Minimal Inhibitory Concentration (MIC) of ZnO MRs and WO_x/ZnO NCs prepared using a different concentration of sodium tungstate dihydrate against Gram-positive and Gram-negative bacteria	149
Table 4.6	Minimal Bactericidal Concentration (MBC) of ZnO MRs and WO_x/ZnO NCs prepared using a different concentration of sodium tungstate dihydrate against Gram-positive and Gram-negative bacteria	150

Table 4.7	Minimal Inhibitory Concentration (MIC) of ZnO MRs and WO_x/ZnO NCs prepared using a different concentration of sodium tungstate dihydrate against Gram-positive and Gram-negative bacteria under 2 h UV light irradiation	151
Table 4.8	Minimal Bactericidal Concentration (MBC) of ZnO MRs and WO_x/ZnO NCs prepared using a different concentration of sodium tungstate dihydrate against Gram-positive and Gram-negative bacteria bacteria under 2 h UV light irradiation	151
Table 4.9	Comparison of structural, optical properties and photocatalytic activity between ZnO, WO_x and ZnO-based nanocomposites	159
Table 4.10	Comparison of MIC between ZnO, WO_x and ZnO-based nanocomposites against Gram-positive and Gram-negative bacteria (sample size, n = 3)	159
Table 4.11	Comparison of MBC between ZnO, WO_x and ZnO-based nanocomposites against Gram-positive and Gram-negative bacteria (sample size, n = 3)	160
Table 4.12	Comparison of MIC between ZnO, WO_x and ZnO-based nanocomposites against Gram-positive and Gram-negative bacteria under 2 h UV light irradiation (sample size, n = 3)	160
Table 4.13	Comparison of MBC between ZnO, WO_x and ZnO-based nanocomposites against Gram-positive and Gram-negative bacteria under 2 h UV light irradiation (sample size, n = 3)	161

LIST OF FIGURES

		Page
Figure 1.1	The number of publications related to semiconductor nanoparticles based on photocatalysts (Dimensions, 2018).	2
Figure 2.1	River water quality trend in Malaysia between years 2006 to 2015 (Compendium of Environment Statistics, 2015).	12
Figure 2.2	SEM micrographs of (a) *B. subtilis* (Samarakoon et al., 2012), (b) *S. aureus* (Cui et al., 2015b), (c) *E. coli* (Lv et al., 2014) and (d) *P. aeruginosa* (Kalle et al., 2014).	14
Figure 2.3	Molecular structures of RhB (Lin et al., 2017).	16
Figure 2.4	Bandgaps and band edges positions of some common semiconductor photocatalysts (Zhang et al., 2012).	19
Figure 2.5	Schematic of band edges position and photocatalytic reaction mechanism of ZnO (Feng et al., 2014).	20
Figure 2.6	Proposed mechanisms of antibacterial activity of ZnO (Hu et al., 2007).	23
Figure 2.7	Schematic diagrams of the cell walls of Gram-positive bacteria and Gram-negative bacteria (Murphy et al., 2007).	25
Figure 2.8	Various types of ZnO crystal structures (a) cubic rocksalt, (b) cubic zinc blende and (c) hexagonal wurtzite structure (shaded grey spheres: Zn atoms and black spheres: O atoms) (Yogamalar and Bose, 2013).	32
Figure 2.9	Schematic illustration of the ZnO hexagonal wurtzite in (a) rod-like structure (Skompska and Zarębska, 2014) and (b) disk-like structure (Hussain et al., 2014).	33
Figure 2.10	Model of WO_x crystal structure: (a) WO_2 and (b) γ-WO_3 illustrated by a 3D network of WO_6 octahedra (Gray) (Kaiser et al., 2017).	35
Figure 2.11	Combination of semiconductor photocatalyst (a) Type I and (b) Type II.	36
Figure 2.12	ZnO nanoparticles with various morphology synthesized by solution route (a) ZnO nanoflowers (Cunha and Souza, 2013), (b) ZnO nanodisks (Yousefi et al., 2015), (c) ZnO nanowires (Hu et al., 2007), (d) ZnO nanorods (Hartini et al., 2016) and (e) ZnO nanoneedles (Chang and Chen, 2007).	39

Figure 2.13	WO_x nanoparticles with various morphology synthesized by solution route (a) WO_3 nanoribbon (Gu et al., 2006), (b) WO_3 nanobelts (Song et al., 2006), (c) WO_3 nanowires (Cai et al., 2015), (d) WO_3 nanoplate (Su et al., 2010) and (e) WO_3 nanotube (Zhao and Miyauchi, 2009).	40
Figure 2.14	MIC values of CuO against *E. coli* using broth microdilution method (Ananth et al., 2015).	43
Figure 2.15	Bacteria growth in the presence of (a) commercial and (b) as-synthesized ZnO nanoparticles (Singh and Nanda, 2013).	44
Figure 3.1	Flowchart of the research project.	52
Figure 3.2	Flowchart of synthesis of ZnO MRs.	57
Figure 3.3	Flowchart of synthesis of ZnO NDs.	58
Figure 3.4	Flowchart of synthesis of WO_x NPs.	59
Figure 3.5	Flow chart of synthesis of WO_x/ZnO NCs.	60
Figure 3.6	Schematic diagrams showing the example layout of the (a) Minimal Inhibitory concentration (MIC) and (b) Minimal Bactericidal Concentration (MBC) plates and dishes used in the antibacterial susceptibility assay.	68
Figure 3.7	Flowchart of antibacterial study using semiconductor photocatalyst.	69
Figure 4.1	XRD patterns of specimen A (ZnO MRs) and specimen B (ZnO NDs).	71
Figure 4.2	FESEM images of (a) ZnO MRs and (b) ZnO NDs. The interfaces of the polar surface (highlight in dotted square boxes) were shown in the image.	73
Figure 4.3	Average thickness of ZnO NDs.	77
Figure 4.4	EDX analysis of (a) ZnO MRs and (b) ZnO NDs.	74
Figure 4.5	TEM images of (a) ZnO MRs and (b) ZnO NDs.	74
Figure 4.6	HRTEM images of (a) ZnO MRs and (b) ZnO NDs.	75
Figure 4.7	SAED patterns of (a) ZnO MRs and (b) ZnO NDs.	76
Figure 4.8	TEM image and EDX mapping of ZnO MRs (b) Zn element and (c) O element.	76
Figure 4.9	TEM image and EDX mapping of ZnO NDs (b) Zn element, (c) O element and (d) Al element.	77

Figure 4.10	FTIR spectra of ZnO MRs and ZnO NDs.	78
Figure 4.11	Room temperature PL spectrum of (a) ZnO MRs and (b) ZnO NDs.	80
Figure 4.12	(a) Proposed growth mechanism of ZnO NRs and (b) nucleation and formation of ZnO MRs.	82
Figure 4.13	Proposed growth mechanism of ZnO flower.	83
Figure 4.14	Proposed growth mechanism of ZnO NDs.	84
Figure 4.15	UV-Vis spectra of photodegraded RhB solution under UV light irradiation (a) No ZnO photocatalyst, (b) ZnO MRs, (c) ZnO NDs and (d) shift of characteristic absorbance peak of RhB.	87
Figure 4.16	Photodegradation efficiency, (b) pseudo first-order kinetics and (c) degradation rate constants of RhB by ZnO MRs and ZnO NDs under UV light irradiation.	89
Figure 4.17	UV-Vis spectra for photodegradation of RhB solution under visible light irradiation by (a) ZnO MRs, (b) ZnO NDs and (c) shift of characteristic absorbance peak of RhB.	92
Figure 4.18	(a) Photodegradation efficiency, (b) pseudo first-order kinetics and (c) degradation rate constants of RhB over ZnO MRs and ZnO NDs under visible light irradiation.	93
Figure 4.19	Scavenger tests on the photodegradation efficiency of RhB solution by (a) ZnO MRs and (b) ZnO NDs under UV light irradiation.	95
Figure 4.20	Schematic of photodegradation mechanism of RhB dye by ZnO.	95
Figure 4.21	Minimal Inhibitory Concentration (MIC) scoring using ZnO MRs, ZnO NDs and WO_x NPs against Gram-positive and Gram-negative bacteria in two different conditons: (a) *B. subtilis* – without UV, (b) *B. subtilis* – 2 h UV, (c) *S. aureus* – without UV, (d) *S. aureus* – 2 h UV, (e) *E. coli* – without UV, (f) *E. coli* – 2 h UV, (g) *P. aeruginosa* – without UV, and (h) *P. aeruginosa* – 2 h UV.	100
Figure 4.22	Minimal Bactericidal Concentration (MBC) scoring using ZnO MRs against Gram-positive and Gram-negative bacteria in two different conditons: (a) *B. subtilis* – without UV, (b) *B. subtilis* – 2 h UV, (c) *S. aureus* – without UV, (d) *S. aureus* – 2 h UV, (e) *E. coli* – without UV, (f) *E. coli* – 2 h UV, (g) *P. aeruginosa* – without UV, and (h) *P. aeruginosa* – 2 h UV.	101

Figure 4.23	Minimal Bactericidal Concentration (MBC) scoring using ZnO NDs against Gram-positive and Gram-negative bacteria in two different conditons: (a) *B. subtilis* – without UV, (b) *B. subtilis* – 2 h UV, (c) *S. aureus* – without UV, (d) *S. aureus* – 2 h UV, (e) *E. coli* – without UV, (f) *E. coli* – 2 h UV, (g) *P. aeruginosa* – without UV, and (h) *P. aeruginosa* – 2 h UV.	102
Figure 4.24	Cell wall and plasma membrane compositions of (a) Gram-positive bacteria and (b) Gram-negative bacteria.	105
Figure 4.25	XRD pattern of specimen C (WO_x NPs), which consisted of WO_2 and WO_3 crystal phases.	107
Figure 4.26	(a) FESEM image under 30 kX magnification and (b) EDX analysis of WO_x NPs.	108
Figure 4.27	(a) TEM image, (b) HRTEM image and (c) SAED image of WO_2 NPs.	110
Figure 4.28	EDX mapping of WO_x NPs.	111
Figure 4.29	FTIR spectra of WO_x NPs.	112
Figure 4.30	Photoluminescence (PL) spectra of WO_x NPs.	113
Figure 4.31	UV-Vis spectra for photodegradation of RhB solution under (a) UV light irradiation and (b) visible light irradiation over WO_x.	115
Figure 4.32	(a) Photodegradation efficiency between UV light and visible light irradiation, (b) pseudo first-order kinetics under UV light irradiation, (c) pseudo first-order kinetics under visible light irradiation and (d) degradation rate constants of RhB over WO_x under UV light irradiation.	118
Figure 4.33	Scavenger test on the photodegradation efficiency of RhB solution over WO_x under UV light irradiation.	119
Figure 4.34	Schematic of photocatalyst mechanism and band potentials of WO_x NPs.	120
Figure 4.35	Minimal Bactericidal Concentration (MBC) scoring using WO_x NPs against Gram-positive and Gram-negative bacteria in two different conditons: (a) *B. subtilis* – without UV, (b) *B. subtilis* – 2 h UV, (c) *S. aureus* – without UV, (d) *S. aureus* – 2 h UV, (e) *E. coli* – without UV, (f) *E. coli* – 2 h UV, (g) *P. aeruginosa* – without UV, and (h) *P. aeruginosa* – 2 h UV.	123
Figure 4.36	XRD patterns of ZnO MRs and WO_x/ZnO NCs prepared using a different concentration of sodium tungstate dihydrate.	127

Figure 4.37	FESEM images of (a) ZnO MRs, and WO_x/ZnO NCs prepared using different concentration of sodium tungstate dihydrate, (b) 0.04 M, (c) 0.08 M, (d) 0.10 M and (e) 0.20 M. The interfaces of the polar surface (highlight in dotted square boxes) and the tips with pits (highlight in dotted circles) were shown in the image.	128
Figure 4.38	(a) Average length and diameter and (b) aspect ratio of ZnO MRs and WO_x/ZnO NCs prepared using a different concentration of sodium tungstate dihydrate.	129
Figure 4.39	EDX spectrum of (a) ZnO MRs, (b) WO_x/ZnO NCs prepared using 0.20 M of sodium tungstate dihydrate and (c) W at.% vs concentration of sodium tungstate dihydrate.	131
Figure 4.40	(a-b) TEM images, (c) HRTEM image and (d) SAED image of WO_x/ZnO NCs prepared using 0.20 M of sodium tungstate dihydrate.	132
Figure 4.41	(a) TEM image, EDX mapping of (b) W, (c) Zn and (d) O elements of WO_x/ZnO NCs prepared using 0.20 M of sodium tungstate dihydrate.	133
Figure 4.42	FTIR spectra of ZnO MRs and WO_x/ZnO NCs prepared using a different concentration of sodium tungstate dihydrate.	135
Figure 4.43	(a) RTPL spectra and (b) I_{UV}/I_{Vis} ratio of ZnO MRs and WO_x/ZnO NCs prepared using a different concentration of sodium tungstate dihydrate.	136
Figure 4.44	Schematic of formation of WO_x/ZnO NCs from pre-synthesized ZnO MRs to the deposition of WO_x in the form of particles (Gray: ZnO and purple: WO_x).	137
Figure 4.45	UV-Vis spectra for photodegradation of RhB solution under UV light irradiation by (a) ZnO MRs and (b) WO_x/ZnO NCs prepared using 0.04 M sodium tungstate dihydrate.	138
Figure 4.46	(a) Photodegradation efficiency, (b) pseudo first-order kinetics and (c) degradation rate constants of RhB by ZnO MRs and WO_x/ZnO NCs prepared using 0.04 M sodium tungstate dihydrate under UV light irradiation.	140
Figure 4.47	UV-Vis spectra for photodegradation of RhB solution under visible light irradiation over the (a) ZnO MRs and (b) WO_x/ZnO NCs prepared using 0.04 M sodium tungstate dihydrate.	141

Figure 4.48	(a) Photodegradation efficiency, (b) hypsochromic shift of maximum adsorption peak, (c) pseudo first-order kinetics and (d) degradation rate constants of RhB over ZnO MRs and WO_x/ZnO NCs prepared using 0.04 M sodium tungstate dihydrate under visible light irradiation.	144
Figure 4.49	Scavenger test on the photodegradation efficiency of RhB solution over WO_x/ZnO NCs with 0.04 M sodium tungstate dihydrate under UV light irradiation.	145
Figure 4.50	(a) UV-Visible absorption spectra of photodegraded BCG solution, (b) photodegradation efficiency of RhB and BCG by WO_x/ZnO NCs with 0.04 M sodium tungstate dihydrate under UV irradiation and molecular structures of (c) RhB and (d) BCG (green: π–π* system and blue: n–π* bonding).	147
Figure 4.51	The band edges' position of WO_x/ZnO NCs in Normal Hydrogen Electrode (NHE).	148
Figure 4.52	Minimal Inhibitory Concentration (MIC) scoring using WO_x/ZnO NCs with diferent concentration of sodium tungstate dihydrate against Gram-positive and Gram-negative bacteria in two different conditons: (a) *B. subtilis* – without UV, (b) *B. subtilis* – 2 h UV, (c) *S. aureus* – without UV, (d) *S. aureus* – 2 h UV, (e) *E. coli* – without UV, (f) *E. coli* – 2 h UV, (g) *P. aeruginosa* – without UV, and (h) *P. aeruginosa* – 2 h UV.	152
Figure 4.53	Minimal Bactericidal Concentration (MBC) scoring using WO_x/ZnO NCs against Gram-positive and Gram-negative bacteria in two different conditons: (a) *B. subtilis* – without UV (0.04, 0.08 M), (b) *B. subtilis* – without UV (0.10, 0.20 M), (c) *B. subtilis* – 2 h UV (0.04, 0.08 M), (d) *B. subtilis* – 2 h UV (0.10, 0.20 M), (e) *S. aureus* – without UV (0.04, 0.08 M), (f) *S. aureus* – without UV (0.10, 0.20 M), (g) *S. aureus* – 2 h UV (0.04, 0.08 M), (h) *S. aureus* – 2 h UV (0.10, 0.20 M).	153
Figure 4.54	Minimal Bactericidal Concentration (MBC) scoring using WO_x/ZnO NCs against Gram-positive and Gram-negative bacteria in two different conditons: (a) *E. coli* – without UV (0.04, 0.08 M), (b) *E. coli* – without UV (0.10, 0.20 M), (c) *E. coli* – 2 h UV (0.04, 0.08 M), (d) *E. coli* – 2 h UV (0.10, 0.20 M), (e) *P. aeruginosa* – without UV (0.04 M), (f) *P. aeruginosa* – without UV (0.10 M), (g) *P. aeruginosa* – 2 h UV (0.04 M), (h) *P. aeruginosa* – 2 h UV (0.10 M).	154

LIST OF ABBREVIATIONS

AOP	Advanced oxidation process
ATCC	American type culture collection
B. subtilis	*Bacillus subtilis*
BCG	Bromocresol green
BET	Brunauer–Emmett–Teller
BHI	Brain heat infusion broth
BOD	Biochemical oxygen demand
CB	Conduction band
DI	Deionized water
DNA	Deoxyribonucleic acid
DOE	Department of environment
E. coli	*Escherichia coli*
EDX	Energy Dispersive X-ray Spectroscopy
FDA	Food and drug administration
FESEM	Field Emission Scanning Electron Microscopy
FETs	Field effect transistors
FTIR	Fourier Transform Infrared Spectroscopy
GRAS	Generally recognized as safe
HCP	Hexagonal-close-pack
HRTEM	High-Resolution Transmission Electron Microscopy
ICDD	International centre for diffraction data

ICU	Intensive care units
LEDs	Light-emitting diodes
LPS	Lipopolysaccharides
MBC	Minimal Bactericidal Concentration
MHA	Mueller hinton agar
MHB	Mueller hinton broth
MIC	Minimal Inhibitory Concentration
NBE	Near-band-edge emission
NCs	Nanocomposites
NDs	Nanodisks
NH_3-N	Ammonia-nitrogen
NHE	Normal hydrogen electrode
NPs	Nanoparticles
NWQS	National water quality standard
P. aeruginosa	*Pseudomonas aeruginosa*
PE	Photodegradation efficiency
PLD	Pulsed laser deposition
RhB	Rhodamine B
ROS	Reactive oxygen species
RTPL	Room Temperature Photoluminescence
S. aureus	*Staphylococcus aureus*
SAED	Selected Area Electron Diffraction

MRs	Submicron rods
SS	Suspended solids
TEM	Transmission Electron Microscopy
UV-Vis	Ultraviolet-Visible Spectroscopy
UVA	Ultraviolet A
VB	Valence band
WQI	Water quality index
XRD	X-ray Diffraction

LIST OF SYMBOLS

E_g	Bandgap energy
λ	Lamda
Δk_{app}	The apparent first order first constant

SINTESIS BAHAN NANO ZnO, ZARAH NANO WO_x DAN KOMPOSIT NANO WO_x/ZnO UNTUK PERENCATAN PERTUMBUHAN BAKTERIA DAN PENGURAIAN PEWARNA ORGANIK

ABSTRAK

Rawatan air kumbahan dengan menggunakan zarah semikonduktor terutamanya zarah nano ZnO merupakan salah satu pendekatan alternatif dan ekonomi. Tetapi, fotodegradasi untuk bahan pencemar organik bagi zarah nano ZnO adalah agak kurang baik disebabkan penggabungan elektron-*hole* yang pantas semasa fotogenerasi. Di samping itu, aktiviti antibakteria yang dilaporkan daripada pelbagai kumpulan penyelidikan selalu mengelirukan dan bertentangan. Kajian ini bertujuan untuk meningkatkan prestasi fotokatalitik untuk zarah nano ZnO dari perspektif morfologi dan gandingan. Dalam kajian ini, rod sub-mikron ZnO (46.19 %) telah menunjukkan kecekapan fotodegradasi yang lebih baik daripada disk nano ZnO (21.47 %) selepas radiasi sinaran UV selama 75 minit. Kecekapan fotodegradasi rod sub-mikron ZnO telah menunjukkan sedikit peningkatan dengan mengendapan semikonduktor bernilai jurang kecil (zarah nano WO_x). Kecekapan fotodegradasi komposit nano WO_x/ZnO telah mencapai 48.38 % di bawah sinaran UV. Aktiviti antibakteria zarah nano diuji dengan menggunakan *antibacterial susceptibility assay* dan sinaran UV. Berdasarkan keputusan tersebut, rod sub-mikron ZnO dan komposit nano WO_x/ZnO telah menunjukkan prestasi antibakteria yang lebih baik terhadap bakteria Gram-positif (*Bacillus subtilis* dan *Staphylococcus aureus*) berbanding bakteria Gram-negatif (*Escherichia coli* dan *Pseudomonas aeruginosa*). Kesan perencatan bakteria dengan menggunakan zarah-zarah adalah bergantung kepada jenis bakteria, dan hanya *Escherichia coli* yang sensitif terhadap kehadiran WO_3.

SYNTHESIS OF ZnO NANOMATERIALS, WO_x NANOPARTICLES AND WO_x/ZnO NANOCOMPOSITES FOR INHIBITION OF BACTERIAL GROWTH AND ORGANIC DYES REMOVAL

ABSTRACT

Waste water treatment using wide bandgap semiconductor particles, in particular the ZnO nanoparticles, is one of the alternative and economical approach. However, the photodegradation of organic pollutants by ZnO nanoparticles is relatively poor due to fast recombination of photogenerated electron-holes. In addition, the antibacterial activities reported from various research groups were often confusing and contradicting. The present study aimed to improve the photocatalytic performance of ZnO nanoparticles from the morphology and coupling perspectives. In this project, the ZnO submicron rods (46.19 %) demonstrated better photodegradation efficiency than ZnO nanodisks (21.47 %) after 75 minutes of ultraviolet light irradiation. The photodegradation efficiency of ZnO submicron rods was improved slightly by depositing narrow bandgap semiconductor (WO_x nanoparticles). The photodegradation efficiency of WO_x/ZnO nanocomposites achieved 48.38 % under UV irradiation. These nanoparticles were tested for their antibacterial activity using antibacterial susceptibility assay without and with UV light irradiation. Based on the results, both ZnO submicron rods and WO_x/ZnO nanocomposites displayed better antibacterial performance against Gram-positive bacteria (*Bacillus subtilis* and *Staphylococcus aureus*) than Gram-negative bacteria (*Escherichia coli* and *Pseudomonas aeruginosa*), the effectiveness of inhibition on bacteria by these particles were bacteria-type dependent, and only *Escherichia coli* was sensitive to the presence of WO_3.

CHAPTER ONE

INTRODUCTION

1.1 Research background

Advanced oxidation process (AOP) based on semiconductor materials have been extensively studied as an environmental remedy for wastewater treatment particularly in microbial disinfection (Ibănescu et al., 2014) and organic pollutants removal (Thein et al., 2016). In this process, the photocatalytic activity takes place on the surface of the semiconductor photocatalysts upon activation of sunlight or other light sources with energy greater than the bandgap of semiconductor (Lopes et al., 2011, Pyrgiotakis and Sigmund 2008, Gulyas, 2014). This approach is attractive because it incurs, low setup cost, low operational cost as the chemical reactions can be triggered by sunlight, less harmful by-products such as water and carbon dioxide (Yu et al., 2011) and eco-friendly as it is less toxic to the environment (Ibhadon and Fitzpatrick, 2013).

Attributed to above mentioned advantages, AOP based on semiconductor materials have become research focus as compared to conventional techniques such as ion exchange (Suteu et al., 2001), coagulation (Oncel et al., 2013), adsorption (Lee et al., 2006) and membrane processes (Jirankova et al., 2010). This is evidenced by the increasing publications from the year 2008 to 2017 as shown in Figure 1.1 (Dimensions, 2018). Various types of semiconductor nanoparticles were produced by researchers. Typical photocatalysts of semiconductor nanoparticles are titanium dioxide (TiO_2) nanoparticles (Long et al., 2006), zinc oxide (ZnO) nanorods (Thein et al., 2016), manganese dioxide (MnO_2) nanotubes (Chan et al., 2016), tin dioxide (SnO_2) nanoparticles (Omar et al., 2016) and iron oxide (Fe_2O_3) nanoparticles

(Belkhedkar et al., 2016). These nano-sized particles displayed novel structural, optical, electronic and chemical properties as compared with bulk particles (Yogamalar et al., 2013). In addition, the nanoparticle is better than the bulk particles as it provides a large surface area to volume ratio (Sirelkhatim et. al, 2015, Rajendar et. al, 2014, Stoimenov et al., 2002). The large surface area is needed for the absorption-photodegradation process in organic pollutants removal and as an effective antibacterial agent. In fact, Swetha and Nalini (2013) reported that nano-Bi_4TaO_8Cl nanoparticles (95 %) have higher photodegradation efficiency for Congo red dye removal than bulk-Bi_4TaO_8Cl (85 %) in 80 min under UV irradiation.

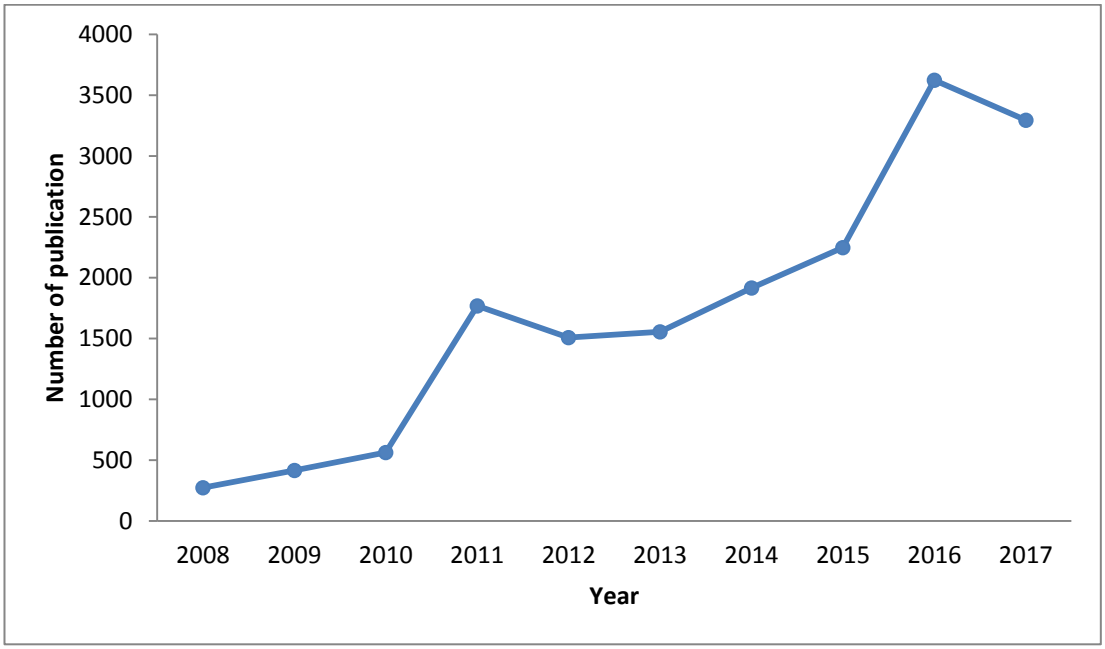

Figure 1.1: The number of publications related to semiconductor nanoparticles based on photocatalysts (Dimensions, 2018).

Bacterial infectious diseases are a great issue in global health perspective. The microbial contaminations in water source are not limited to enteric diseases, but also extend to the other organs. The outbreaks and infections of water-borne pathogens become a health hazard to human. Semiconductor particles display effective non-targeted disinfections over a wide range of microorganisms. This unique characteristic is enhanced by their high specific surface area and strong adsorption ability toward reactants. Some studies showed that nanomaterial could kill eukaryotic cells or inhibit the growth of prokaryotic cells due to cytotoxicity (Long et al., 2006, Magrez et al., 2006). In addition, semiconductor nanoparticles can be designed as pathogen control in clinical care application. The recent advancement in the field of semiconductor nanoparticles has led to a new application in the food sector. In this case, the nanoparticles are used to improve hygiene and to reduce microbial cross-contamination from food contact and non-food contact surfaces that might cause severe foodborne outbreaks (Yemmireddy and Hung, 2017).

TiO_2 is the most extensively studied semiconductor photocatalysts in the past decades due to its excellent photocatalytic behaviour (Zhao et al., 2012), non-toxicity (Lan et al., 2013), good chemical stability (Pant et al., 2013) and inexpensive (Firdaus et al., 2012). TiO_2 photocatalysts were used for organic pollutants removal (Lan et al., 2013), drinking water treatment (McCullagh et al., 2007), antibacterial agent (Xing et al., 2012) and antifungal agent (Darbari et al., 2011). Generally, three different polymorphs of TiO_2 could be found in nature, i.e. anatase, rutile and brookite phases. Different crystal phases demonstrated different effectiveness in removal of organic pollutants and antibacterial effect. It was reported that TiO_2 in the anatase and rutile forms showed good photocatalytic efficiency. Some researchers suggested that this could be attributed to the bandgap of the anatase phase of 3.2 eV

which was responded to UVA or near-UV range ($\lambda < 387$ nm), whereas the bandgap of the rutile phase of 3.0 eV has extended the photo-excitation wavelength into visible light range (410 nm) (Ibhadon and Fitzpatrick, 2013). In addition, anatase phase of TiO_2 demonstrated excellence photocatalytic detoxification due to the high rate of hole trapping and longer lifetime at excited state (Bahnemann et al., 1993), while rutile has quick electron-hole pair recombination (Visai et al., 2011).

Although ZnO has similar optical and photocatalytic properties as compared to TiO_2 (see Table 1.1), it is relatively less frequent studied by researchers. ZnO is an inorganic semiconductor which normally appears in white colour powder. It is a compound semiconductor (II-VI group); with Zn in group two and O in group six in the periodic table. The pH level of ZnO is within 7-8, indicating that it is a safe and environmentally friendly material. It has a wide bandgap (3.2-3.37 eV) and large excitation binding energy (~ 60 meV) at room temperature (Shah et al., 2014). Thus, it is a potential candidate for the fabrication of high-performance optoelectronic devices such as field effect transistors (FETs) (Fan and Lu, 2005), laser (Look and Claflin, 2004) and light-emitting diodes (LEDs) (Manoharan et al., 2015). Besides, it has good piezoelectricity property which could be used to fabricate a piezoelectric generator (Lu et al., 2017). Lastly, ZnO shows a very strong ionic bonding between Zn and O, which is suitable to be used as photocatalyst due to its longer durability and good thermal stability (Hatamie et al., 2015).

Table 1.1: A comparison between ZnO and TiO_2 properties (Wei et al., 2015, Gorospe and Herrera, 2017)

	Properties	**ZnO**	**TiO_2**
1	Type of bandgap	Direct bandgap	Indirect bandgap
2	Bandgap energy (eV)	3.2-3.37	Anatase (3.2) Rutile (3.0)
3	Wavelength (nm)	368-388	Anatase (387) Rutile (413)
4	Price (RM/kg)	330.00	377.50

The photodegradation mechanism of organic pollutants of ZnO is identical as compared to TiO_2. However, it was reported that ZnO was able to absorb a larger fraction of solar spectrum than TiO_2, particularly in visible light range (Behnajady et al., 2006). Thus, ZnO showed a higher efficiency of reactive species generation and a better in photoinduced electron and hole separation than TiO_2 (Sapkota et al., 2011). Furthermore, it is also cheaper than TiO_2. The cost of ZnO powder is RM 330.00/kg and TiO_2 powder is RM 377.50/kg. Thus, ZnO is a potential replacement for TiO_2 as a photocatalyst (Sakthivel et al., 2003).

The other visible light driven photocatalysts such as MnO_2 nanotubes (Chan et al., 2015), Fe_2O_3 nanoparticles (Belkhedkar et al., 2016), porous carbon nitride (Zhou et al., 2018a) and AgI/$Bi1_2O_{17}C_{l2}$ (Zhou et al., 2018b) demonstrated good photocatalysts for organic pollutants removal. Amongst these semiconductor nanoparticles, tungsten oxide (WO_x) has a better absorption in visible light irradiation due to its small bandgap. Besides, it has high oxidation power of valence band holes (Sangeeta et al., 2015). Thus, it has been used as photocatalyst. The cost of WO_x powder is RM 4100/kg, yet it still consider lower cost than other narrow bandgap semiconductor materials (Merck, 2018). In fact, a yield of 19 % was obtained using a Ce–WO_x photocatalyst in photocatalytic water splitting process for hydrogen production (Patel et al., 2013). A WO_x based composite demonstrated high

photodegradation on phenol and methyl orange (Karácsonyi et al., 2013). As compared to the widely studied TiO_2 and ZnO as UV light driven photocatalysts, the photocatalytic performance of WO_x nanoparticles in organic dye removal and its antibacterial property are relatively less investigate although some works had been reported by Szilágyi et al. (2012), Wicaksana et al. (2014), Dong et al. (2017) and Vinesh et al. (2018).

1.2 Problem statement

As far as ZnO photocatalyst is concerned, the most studied nanostructure is ZnO nanorods (NRs). This is because ZnO NRs are the easiest synthesized nanostructure, attributed to their preferred [0001] growth direction of wurtzite crystal structure (Wang, 2004a). The antibacterial effect of ZnO NRs has been widely studied by Tam et al. (2008), Rago et al. (2014), Wang et al. (2004), Jansson et al. (2012) and Luo et al. (2013), whereas the photocatalytic performances for organic compounds removal of ZnO NRs were reported by Leow et al. (2015), Chouchene et al. (2016), Al-Sabahi et al. (2016), Kuriakose et al. (2014) and Azam and Babkair (2014).

However, ZnO is known for its diverse nanostructures (Wang, 2004b). Various ZnO nanostructures such as nanorods (Eskandari et al., 2011), nanosprings (Gao and Wang, 2005), nanohelics (Zhou et al., 2017), nanoflowers (Sharma et al., 2015) and nanobelt (Wang et al., 2007) were synthesized by selective synthesis conditions or by foreign catalysts. These ZnO nanostructures have (i) different surface area to volume ratio and (ii) expose different crystal planes. These two properties could affect the photocatalytic performance of ZnO nanostructures for organic pollutants removal and inactivation of bacteria. Thus, the photocatalytic

performance of ZnO nanostructures, particularly nanorods and nanodisks (with the large polar surface) are worthy of study.

Next, the use of wide bandgap semiconductor photocatalysts such as ZnO has its limitations. Attributed to its wide bandgap (E_g = 3.2-3.37 eV), ZnO only responses to optical excitation source, e.g. UV light that has excitation energy larger than its bandgap. Poor photocatalytic removal efficiency was reported by Nguyen et al. (2018) if performed under visible light. In fact, it took 3 h in order to photodegrade 250 ml of 10^{-5} mol L^{-1} methylene blue (MB) dye solution under visible light ($\Delta k_{app} = 0.095\ h^{-1}$). Thus, the removal efficiency of organic pollutants and bacteria inactivation using ZnO photocatalyst under sunlight is not optimum as the solar spectrum consists of only ~ 4% of UV light and 46% of visible light. Therefore, ZnO photocatalyst is difficult to be used in large scale for wastewater treatment.

Appropriate tailoring of wide bandgap semiconductor photocatalysts could improve the above weakness. There are a few approaches have been widely adopted to improve the photocatalytic performance of these materials.

(i) By prolonging the recombination duration of photogenerated electron-hole charge carriers. This could be achieved by (a) doping with transition metal ions, e.g. Mn (Rekha et al., 2010), Co (Nair et al., 2011) or non-metal element, e.g. N- (Lavand and Malghe, 2015). The dopants could either induce energy levels in the bandgap of ZnO (Mia et al., 2017) or reduce the bandgap of ZnO so as it is responsive towards visible light region (Ahmad et al., 2013); (b) deposition of noble metals, e.g. gold (Castillejos et al., 2012) and (c) co-doping with different element, e.g. Ce-Ag-ZnO (Subash et al., 2012).

(ii) By shifting the optical absorbance of ZnO into the visible wavelength via coupling with narrow bandgap semiconductor material, e.g. SnO_2/ZnO (Zhu et al., 2015), α-Fe_2O_3/ZnO (Xie et al., 2015) and ZnO/CdS (Wang et al., 2016).

In this work, ZnO submicron rods (MRs), ZnO nanodisks (NDs), WO_x nanoparticles (NPs) and WO_x/ZnO nanocomposites (NCs) were produced using a solution approach. As compared with ZnO MRs, ZnO NDs consist of large (002) polar surface, which terminated either by positively charged $–Zn^{2+}$ ions or by negatively charged $–O^{2-}$ ions. This unique property of ZnO NDs could affect their photocatalytic activities. The WO_x NPs were selected in this project as WO_x is a narrow bandgap semiconductor (Eg = 2.4-2.8 eV), which might improve the photocatalytic response of WO_x/ZnO NCs under visible light. The photodegradation efficiency of organic dyes removal and bacterial susceptibility of these particles were studied and compared. The antibacterial mechanism was elucidated based on the collective results of the study.

1.3 Research objectives and scopes of work

This project is aimed to assess the photocatalytic performance of ZnO particles in organic dyes removal and bacteria inactivation from the perspectives of (i) morphology and (ii) coupling with a narrow bandgap semiconductor (WO_x). To achieve this aim, the following objectives have been formed:

(i) To assess the photocatalytic performance and identify the main reactive species from ZnO MRs, ZnO NDs, WO_x NPs and WO_x/ZnO NCs that responsible for organic dyes removal.

(ii) To understand the antibacterial activity and elucidate the antibacterial mechanism of ZnO MRs, ZnO NDs, WO_x NPs and WO_x/ZnO NCs.

In Stage 1, ZnO MRs, ZnO NDs were synthesized via solution precipitation method. The structural and optical properties of these particles were characterized using X-ray diffraction (XRD) technique, Field Emission Scanning Electron Microscopy (FESEM)/ Energy Dispersive X-ray (EDX) Spectroscopy, Transmission Electron Microscopy (TEM)/ High-Resolution Transmission Electron Microscopy (HRTEM)/ Selected Area Electron Diffraction (SAED), Brunauer–Emmett–Teller (BET), Fourier Transform Infrared Spectroscopy (FTIR), Room Temperature Photoluminescence (RTPL) measurement and UV-Visible (UV-Vis) Spectroscopy. The photocatalytic performances of these particles in the removal of organic dyes were examined. The main reactive species that responsible for the degradation of organic dyes from these particles were determined by scavenger tests. Identification of the main reactive species was important as providing a hint for deducing the mechanism of bacteria inactivation in Stage 2-3. In addition, the antibacterial susceptibility assay was performed on these particles was conducted. Based on these results, ZnO MRs was selected in Stage 3 as the particles performed better in RhB dye removal and inactivation of bacteria.

In Stage 2, the WO_x NPs were produced using sodium tungstate dihydrate and hydrochloric acid via solution precipitation method. The optical and structural properties of WO_x NPs were characterized. Similarly, the photocatalytic performance of WO_x NPs in RhB dye removal and antibacterial were assessed.

In Stage 3, WO_x/ZnO NCs were produced via liquid impregnation method. The pre-synthesized ZnO MRs was dispersed in the solution of sodium tungstate

dihydrate in order to allow deposition of WO_x on the surface of ZnO MRs. The concentration of sodium tungstate was varied in order to increase the amount of deposition of WO_x. The structural, optical and photocatalytic properties of this WO_x/ZnO NCs were studied and compared with ZnO MRs and WO_x NPs.

1.4 Dissertation Outline

This thesis consists of five chapters. Chapter one describes the research background, problem statement, objectives and outline of this research. Chapter two reviews the recent development of semiconductor photocatalysts particularly in organic dyes and antibacterial study. Chapter three provides the details of chemicals and culture media used in this work. The procedures to synthesize ZnO MRs, ZnO NDs, WO_x NPs and WO_x/ZnO NCs also included. The working principles and sample preparation method of key characterization techniques, as well as photocatalytic assays in inactivation of bacterial and RhB dye removal are discussed. Chapter four presents the results of structural, optical and photocatalytic performance of ZnO MRs, ZnO NDs, WO_x NPs and WO_x/ZnO NCs. The photocatalytic mechanisms of these particles in inactivation of bacteria and degradation of RhB dye were discussed. Lastly, Chapter five summarizes the key findings of this research works and recommends future research direction in this field.

CHAPTER TWO

LITERATURE REVIEW

2.1 Introduction

This chapter provides the literature review of ZnO and WO_x as photocatalysts. Section 2.2 gives the overview of water pollution in Malaysia and discusses the major pollutant sources found in untreated water, including bacterial and organic dyes. In Section 2.3, the recent development of water treatment technology is presented. Specifically, mechanism and factors affecting its performance of AOP based on semiconductor photocatalysts are discussed in details as it was used in this project. The general properties and synthesis techniques of ZnO and WO_x nanostructures are discussed in Sections 2.4 and 2.5, respectively. Lastly, the antibacterial susceptibility assay using broth dilution method and other antibacterial assessment techniques are presented in Section 2.6.

2.2 Water pollution in Malaysia

The water pollution of Malaysia is monitored by the Department of Environment (DOE). This agency uses Water Quality Index (WQI) and National Water Quality Standard for Malaysia (NWQS) as a standard to classify the quality of river water. According to DOE, there are three major pollutants that have a great impact on the quality of river water, i.e. ammonia-nitrogen (NH_3-N), biochemical oxygen demand (BOD) and suspended solids (SS). The main sources of NH_3-N are mainly found from domestic sewage and livestock farming; BOD is probability came from the untreated or partially treated sewage and manufacturing industries, and SS is generated from earthworks and land clearing activities. BOD is a measure of

oxygen level in water that being consumed by microorganism. A high BOD indirectly indicates a lot of bacteria are present to decompose the organic waste in the water. Figure 2.1 displays the river water quality of Malaysia from year 2006 to 2015. Although the percentage of polluted rivers has reduced from 58 (10 %) in the year 2006 to 33 (7 %) in the year 2015, the total percentage of polluted and slight polluted rivers is still a main concern, i.e. 42 % (201 rivers out of 477 rivers). More effort is still needed to improve the cleanliness of water river quality as the rivers are the main source of drinking water in Malaysia.

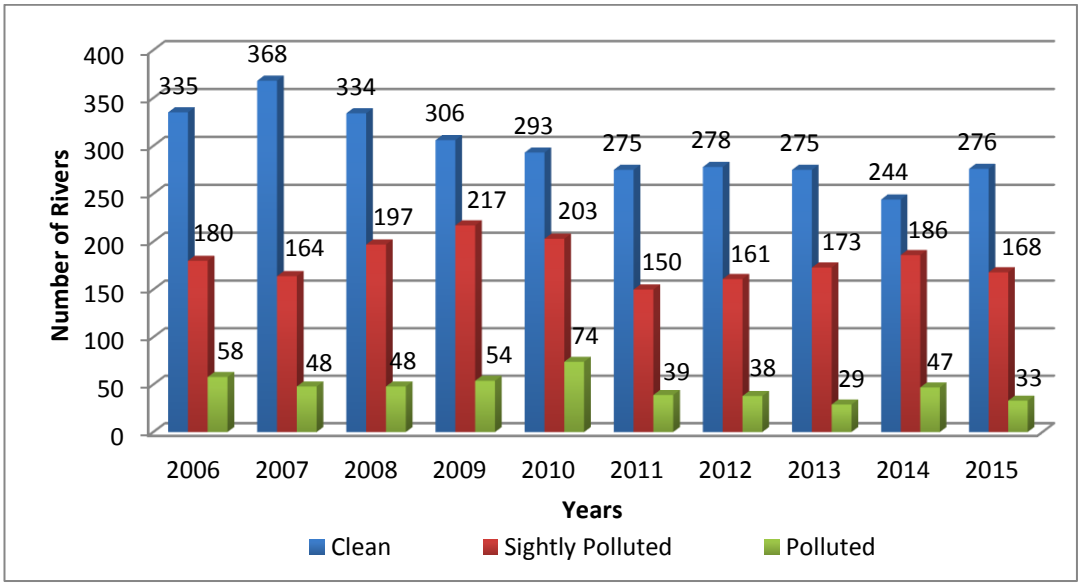

Figure 2.1: River water quality trend in Malaysia between years 2006 to 2015 (Compendium of Environment Statistics, 2015).

Untreated water contains a large amount of organic pollutants, bacteria and other microorganism. Organic pollutants such as dyes from textile or batik industry can cause skin irritation and spread waterborne disease if it is not properly treated. The bacteria quantity of untreated water can be assessed by its coliform bacteria content. These large bacteria could affect internal organ and could be found in the digestive tract of warm-blooded animals or humans. In addition, pathogenic

microorganisms found in untreated water are potential health hazards. The standard of drinking water quality developed by DOE of Malaysia for raw water and treated water is shown in Appendix 1.

2.2.1 Bacterial

Microorganism or bacteria are widely found in untreated water. Generally, these bacteria can be classified into two main categories, i.e. Gram-positive bacteria and Gram-negative bacteria based on the Silhavy et al. (2010) studied. In this research, two common types of Gram-positive bacteria, i.e. *Bacillus subtilis* (*B. subtilis*) and *Staphylococcus aureus* (*S. aureus*) and two common types of Gram-negative bacteria, i.e. *Escherichia coli* (*E. coli*) and *Pseudomonas aeruginosa* (*P. aeruginosa*) were selected. In the recent study, the outcomes of infections found in the worldwide intensive care units (ICU) come from Gram-negative bacteria. Out of 62 % of the isolated bacteria, there are 20 % come from Pseudomonas species and 16 % from Escherichia (Vincent et al., 2009). *B. subtilis* is a Gram-positive bacterium with the size of 4-10 µm as shown in Figure 2.2(a). It is mainly found in soil and gastrointestinal tract of humans (Yoshpe-purer and Golderman, 1987). They are usually detected in drinking-water supplies and diseases may result from the ingestion of these bacteria. *S. aureus* is also a Gram-positive bacterium and arranged in grapelike irregular clusters as shown in Figure 2.2(b). It has spherical shaped strains. It is a non-motile bacterium which mainly found in hair follicles, human skin and nasal membranes of warm-blooded animals. They also can be released through human contact into swimming pools and other recreational waters, hence could be detected in drinking water sources (Guidelines for Drinking-water Quality, 2011). This bacterium might cause diseases such as food poisoning and toxic shock

syndrome (Teh et al., 2016). In contrary, *E. coli* is classified as Gram-negative. As shown in Figure 2.2(c), it has a rod-shaped of about 1 µm long and 0.35 µm wide (Blount, 2015). *E. coli* was presents in large number in the environment, where generally causing severe disease in humans and animals (Lim et al., 2010). Thus, they used as an important indicator for monitoring faecal contamination and verifying water quality. Figure 2.2(d) shows the image of *P. aeruginosa*. It is a non-fermenting Gram-negative bacterium (Morita et al, 2014). *P. aeruginosa* is a common environmental organism that could be discovered in plants, soil, sewage and water. They can cause a wide range of infections such as urinary tract infections, respiratory infections and patients wound.

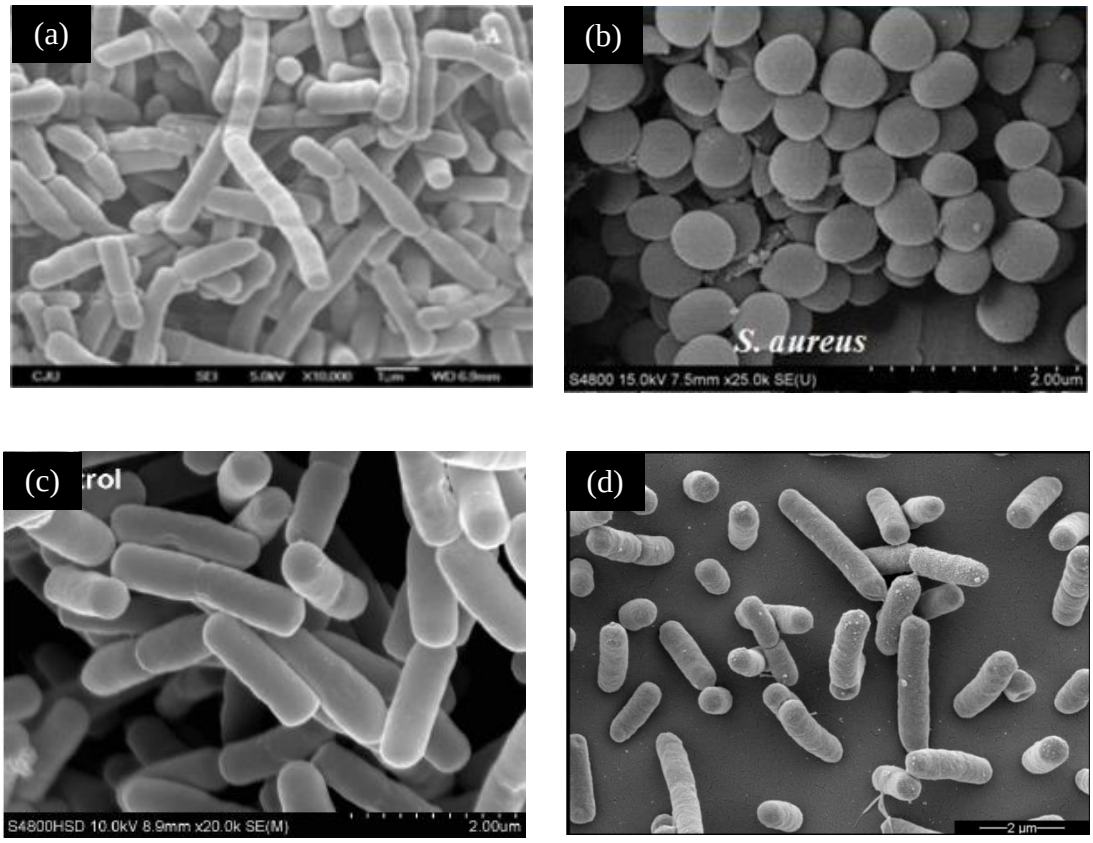

Figure 2.2: SEM micrographs of (a) *B. subtilis* (Samarakoon et al., 2012), (b) *S. aureus* (Cui et al., 2015b), (c) *E. coli* (Lv et al., 2014) and (d) *P. aeruginosa* (Kalle et al., 2014).

2.2.2 Organic dyes

Dyes are one of the main pollutants from textile industry if is discharged into the water system untreated. The dye textile effluent exhibits a high value of pH, strong colouring, high BOD and COD concentration. It also contains different heavy metals and surfactants (McClatchy, 2011). In addition, most of the organic dyes contain aromatic rings, which are toxic to the environment and difficult to degrade due to its stable chemical structures (Mantzavinos and Elefteria, 2004). The different synthetic compounds presented in dye effluent have proven (i) different biological activity in the water and (ii) problematic to the environment with its high toxicity and low biodegradability (Sriram and Reetha, 2015).

Organic dyes contain two major components (i) chromophores and (ii) auxochromes. The common components of chromophores are -C=N-, -C=C-, -C=O-, -N=N-, and $–NO_2$. These components generally have conjugated double bonds. In contrary, auxochromes are –COOH, $–NH_3$, $–SO_3H$ and –OH groups that help to intensify the colour of the chromophore. Depending on the chromophore structures, different groups of organic dyes such as basic dyes, acid dyes, reactive dyes, disperse dyes and solvent dyes can be obtained.

Basic dyes are water-soluble dyes that produced coloured cations in solution. These dyes contain diarylmethane, anthraquinone, triphenylmethane or azo components (Lam et al, 2012). For instance, rhodamine B (RhB) belongs to triphenylmethane family, consisting four N-ethyl groups at either side of the xanthene ring (Yu et al., 2009) as illustrated in Figure 2.3. RhB dye is widely used in textile industry attributed to its high resistance to biological and chemical degradation. However, this becomes an environmental issue if the dye is discharged

into water system untreated. As a very stable chemical compounds, it is going to take a very long duration for degradation. RhB shows a strong intrinsic absorption band in the visible region of wavelength 554 nm. RhB was chosen as the model pollutant in this project due to its stable chemical structure and thus suitable to investigate the photocatalytic performance of ZnO based photocatalysts.

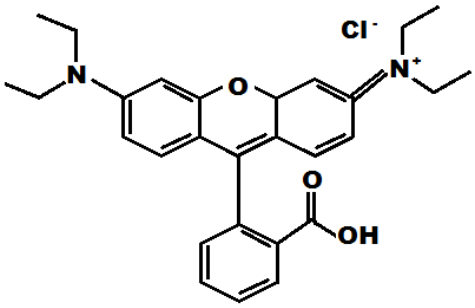

Figure 2.3: Molecular structures of RhB (Lin et al., 2017).

2.3 AOP

Freshwater resources are getting lesser as a result of water pollution caused by the dumping of untreated industrial and domestic wastes. Particularly, these pollutants contained organic pollutants and water-borne pathogens. The organic pollutants and water-borne pathogens in wastewater are toxic to the environment and difficult to degrade or remove in the natural environment due to its stable chemical structures. The organic pollutants have become a health hazard to people after drinking this water. Owing to these reasons, treatment of drinking water to prevent the spreading of infectious diseases is important.

There are some major conventional wastewater treatments processes have been developed to inactivate bacteria and to degrade non-biodegradable dye effluents. These processes are chemical oxidation (Skákalová et al., 2018),

physicochemical wastewater treatment (Frigon et al., 2013), membrane separation process (Strathmann, 1981) and biological waste treatment method (Cardenas et al., 2016). Nevertheless, these techniques for water purification are either high cost as required intensive energy or generating hazardous by-products. Therefore, new wastewater techniques are required for producing drinking water and solving environmental problems.

Amongst new emerging techniques, AOP based on semiconductor photocatalysts has attracted many research attentions in wastewater treatment for the degradation of toxic organic compounds and microbial disinfection in water (Xue et al., 2016). Semiconductor nanoparticles are promising candidates due to its capability to decompose organic pollutants into less harmful compounds and inactivation of bacteria at low cost.

AOP is a chemical approach to treat contaminated water containing residual dyes and microorganisms. It generates highly reactive hydroxyl free radicals to degrade toxic compounds present in wastewater. This can be achieved by using UV/O_3, UV/H_2O_2, UV/Fenton, $UV/O_3/H_2O_2$ or UV/semiconductor photocatalysts. Some of the commonly reported semiconductor photocatalysts are TiO_2 (Zhou et. al, 2006), ZnO (Karunakaran et al, 2010), Fe_2O_3 (Azam et al., 2012) and SnO_2 (Zheng, 2016). The advantages of this approach are energy efficient and able to degrade organic effluents which are structurally stable and difficult to biologically degrade completely.

Photocatalysis involves photochemistry and catalysis. Thus, light with a suitable wavelength and a catalyst are required to accelerate a chemical transformation. In the case of using semiconductor (heterogeneous) photocatalysts,

photoreactions occur at the surface of the semiconductor (Rehman et al., 2009). The photocatalytic performance of various types of wide bandgap semiconductors, e.g. TiO_2 (Hashimoto et al, 2005), ZnO (Qi et al., 2017), zinc sulfide (ZnS) (Zhang et al., 2007) and narrow bandgap semiconductors, e.g. tin selenide (SnSe) (Ashiq et al., 2017), indium antimonide (InSb) (Wu et al., 2014) and lead (II) sulfide (PbS) (Ratanatawanate et al., 2009) have been studied by researchers.

2.3.1 General semiconductor photocatalysis mechanism

Two important conditions need to be considered for an effective photocatalytic process, i.e. (i) the photon energy of light and (ii) the band edges position in the normal hydrogen electrode (NHE) diagram (Mills and LeHunte, 1997).

(i) Photon energy of light

The amount of photon energy needed to generate electron-hole pairs depends on the energy difference (bandgap, E_g) between the valence band (VB) and the conduction band (CB) of a semiconductor material. The photon energy needs to be equal or greater than the bandgap of the semiconductor in order to excite the electrons from VB to CB. No photogenerated electrons and holes could be produced if the photon energy is less than the bandgap, and thus the subsequent photocatalysis process is not possible.

(ii) Band edges position in the NHE diagram

The photogenerated electrons and holes need to have sufficient redox potential in order to produce free radicals. Figure 2.4 displays the schematic of the

band edges positions of some common semiconductor photocatalysts on a redox potential scale (V) versus NHE. For an efficient photocatalysis, the CB should be higher in energy (more negative potential) than the redox potential of $O_2/•O_2^-$ (-0.046 eV vs NHE in order to produce superoxide anion free radicals ($•O_2^-$) and the VB must be lower in energy (more positive potential) than the redox potential $OH^-/•OH$ (1.99 eV vs NHE) in order to produce hydroxyl free radicals (•OH) (Yemmireddy and Hung, 2017).

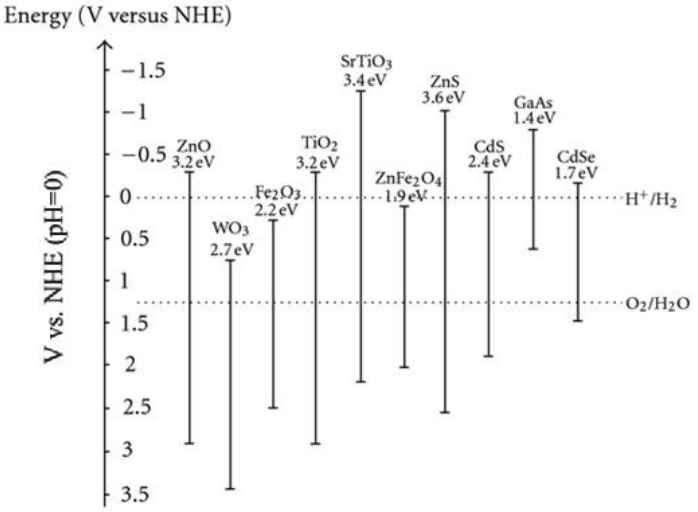

Figure 2.4: Bandgaps and band edges positions of some common semiconductor photocatalysts (Zhang et al., 2012).

If the above two conditions comply, an effective photocatalysis process is expected. For instance, ZnO is one of the widely studied photocatalysts for organic compounds removal and inactivation of bacteria. The photocatalytic mechanism can generally occur in four steps, i.e. (i) charge-carrier production, (ii) charge-carrier trapping, (iii) charge-carrier recombination and (iv) photocatalytic degradation of organic pollutants or inhibition of bacteria and microorganism (Vijayaprasath et al., 2016, Jalal et al., 2010).

(i) Charge-carrier production

As ZnO is a wide bandgap semiconductor (E_g = 3.2-3.37 eV), it only responses to ultraviolet (UV) light but not visible light in order to produce electrons (e^-) in the CB and holes (h^+) in the VB (Equation 2.1) as illustrated in Figure 2.5 (Feng et al., 2014, Dasari et al., 2013, Mala et al., 2016).

$$ZnO + h\nu \rightarrow e^- + h^+ \quad (2.1)$$

(ii) Charge-carrier trapping

As the band edge of VB of ZnO is more positive potential than the redox potential of $OH^-/\bullet OH$ (1.99 eV vs NHE), the photogenerated holes will oxidize the electron donors such as water (H_2O) or hydroxyl ion (OH^-) to produce very reactive oxidizing agent, i.e. •OH as shown in Equation 2.2 and Equation 2.3.

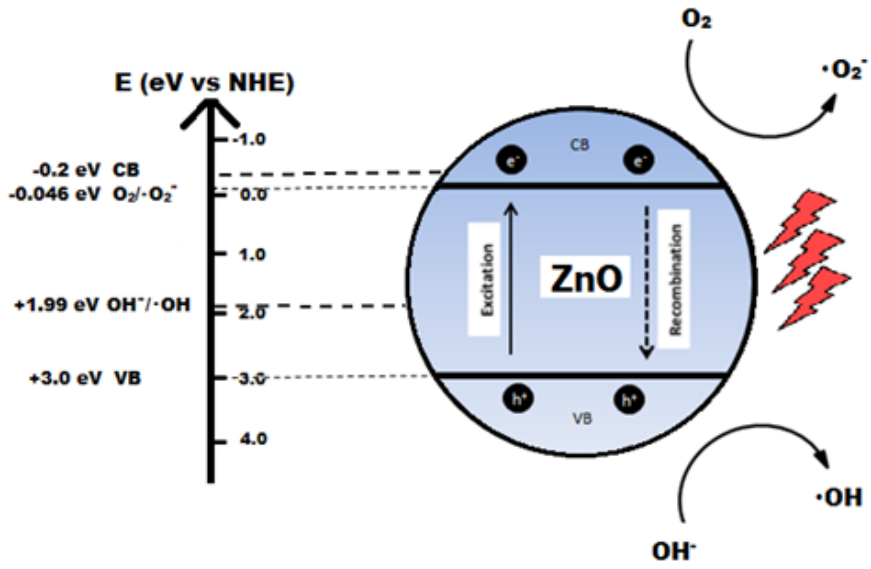

Figure 2.5: Schematic of band edges position and photocatalytic reaction mechanism of ZnO (Feng et al., 2014).

$$h^+ + H_2O \rightarrow \bullet OH + H^+ \quad (2.2)$$

$$h^+ + OH^- \rightarrow \bullet OH \quad (2.3)$$

In contrary, as the CB edge of ZnO is more negative potential than the redox potential of O_2/ $\bullet O_2^-$ (-0.046 eV vs NHE), the photogenerated electrons will react with oxygen (O_2) that absorbed on the photocatalyst and form superoxide radical anion ($\bullet O_2^-$) (Equation 2.4). These $O_2^{\bullet-}$ will react with hydrogen ion (H^+) subsequently in order to form hydroperoxyl radical ($\bullet HO_2$) (Equation 2.5). Next, it will collide with e^- to generate hydroperoxyl anions (HO_2^-) (Equation 2.6). After that, it will react with H^+ to create hydrogen peroxide (H_2O_2) (Equation 2.7). The photogenerated electrons also can react with H_2O_2 to form •OH and OH^- (Equation 2.8).

$$e^- + O_2 \rightarrow \bullet O_2^- \quad (2.4)$$

$$\bullet O_2^- + H^+ \rightarrow \bullet HO_2 \quad (2.5)$$

$$\bullet HO_2 + e^- \rightarrow HO_2^- \quad (2.6)$$

$$HO_2^- + H^+ \rightarrow H_2O_2 \quad (2.7)$$

$$e^- + H_2O_2 \rightarrow OH^- + \bullet OH \quad (2.8)$$

It is also noted that the photogenerated holes can oxidize directly the organic pollutant into H_2O, carbon dioxide (CO_2) and mineral acids.

(iii) Charge-carrier recombination

Recombination of charge carriers is not preferred in the photocatalytic process as it reduces the number of photogenerated holes and electrons which is needed for the generation of reactive oxygen species (ROS). Nevertheless, it is a natural process to occur after optical excitation of semiconductor material. Some of the unreacted electron-hole pairs may relax back to the VB within nanoseconds (Talebian et al., 2011). When the recombination takes places, the input energy might dissipate as heat (phonon) or light (photon) (Equation 2.9) (Zhao, 2012).

$$e^- + h^+ \rightarrow \text{heat/light} \quad (2.9)$$

(iv) Photocatalytic degradation

The photogenerated electron-hole pairs in photocatalytic degradation process have resulted in production of ROS. Consequently, four possible reactive species, i.e. h^+, e^-, $\bullet O_2^-$ and •OH can degrade the organic dyes and inhibit bacteria (Equation 2.10-2.14). In addition, the $\bullet O_2^-$ can further react with H_2O_2 to form OH^-, •OH and singlet oxygen (O_2) (Equation 2.10) (Haja Hameed et al., 2015). The electrons and holes are a strong reducing agent and oxidizing agents, respectively. Thus, these charge carriers can either reduce or oxidize the organic dye (R) into various intermediates ($R^+_{intermediate}$) as shown in Equations 2.11-2.12. The intermediate products will further react with •OH to generate final degradation products, such as CO_2, H_2O and acid minerals (Equation 2.13). The •OH will also react with bacteria cell to inactivate the bacteria (Equation 2.14) (Rizzo, 2009).

$$\bullet O_2^- + H_2O_2 \rightarrow OH^- + \bullet OH + O_2 \quad (2.10)$$

$$\text{Organic dye (R)} + e^- \rightarrow R^+_{intermediate} \quad (2.11)$$

$$\text{Organic dye (R)} + h^+ \rightarrow R^+_{intermediate} \quad (2.12)$$

$$\text{Organic dye (R)} + \bullet OH \rightarrow R^+_{intermediate} \rightarrow CO_2 + H_2O + \text{amino acids} \quad (2.13)$$

$$\text{Bacteria} + \bullet OH \rightarrow \text{inactivation of bacteria} \quad (2.14)$$

2.3.2 Other factors that contributing to the inactivation of bacteria

The ability to inhibit or kill the growth of bacteria, microorganisms and pathogens completely by semiconducting particles was studied by researchers. Several inactivation mechanisms of bacterial by semiconductor particles have been proposed by researchers, involving ROS, destruction interaction of cell membrane

wall, deactivation of the enzyme, leakage of deoxyribonucleic acid (DNA) or contribution of metal ions as illustrated in Figure 2.6 (Hu et al., 2007).

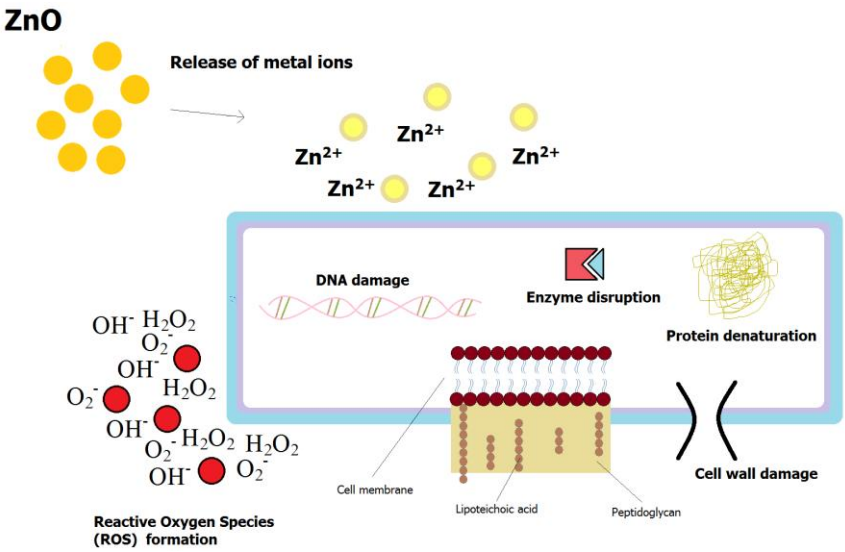

Figure 2.6: Proposed mechanisms of antibacterial activity of ZnO (Hu et al., 2007).

(i) Invasion of reactive oxygen species (ROS)

ROS are chemical intermediates such as •OH, $•O_2^-$ and H_2O_2. The invasion of ROS to cell membrane constituents, i.e. proteins, lipids or DNA is highly toxic to the bacteria (Storz and Imlay, 1999, Kirkinezos and Moraes, 2001, Xia et al., 2006).

Nair et al. (2011) stated that the antibacterial efficiency of metal oxide depended on the generation rate of oxygen-related free radicals such as •OH on its surface. The •OH is the strongest non-selective agents that can react very quickly with aromatic ring compounds and damage virtually almost all type of bio-molecules found in living cells, such as carbohydrates, lipids, proteins, amino acids and DNA (You et al., 2011).

In contrary, $•O_2^-$ is less toxic and the H_2O_2 is considered the weakest oxidizer (Haja Hameed et al., 2015). In fact, Talebian et al (2011) reported that H_2O_2 could

diffuse into the cell membrane as it is less harmful compared to •OH and $•O_2^-$. Nevertheless, H_2O_2, in the presence of $•O_2^-$, is able to produce singlet oxygen which is high toxicity to the bacteria. The damages by $•O_2^-$ and H_2O_2 only can take places on the cell membrane from outside of the bacteria.

A detail studied by Premanathan et al. (2011) revealed that the intracellular oxidative stress induced by ZnO on bacteria cell could lead to oxidative damage of cell membrane. In this case, the damage was proposed mainly attributed to the production of ROS by ZnO during the photocatalytic reaction. When the ROS produced by the ZnO exceeded the tolerance capacity of the cellular antioxidant defense system, the balance between oxidant and the antioxidant process was disturbed, eventually caused bacterial cell force to enter oxidative stress state (Vijayaprasath et al., 2016). The excess of oxidative stress phenomena disrupted the cell membrane integrity due to ZnO and subsequently damage to the cell membrane component and lead to cell death (Dasari et al, 2013). In addition, Li et al. (2012b) studied the average concentrations of ROS produced by different types of metal oxides, i.e. CeO_2 (8.4 ± 0.2 µM), CuO (0 µM), SiO_2 (56.5 ± 2.5 µM), Al_2O_3 (158.5 ± 8.0 µM) and Fe_2O_3 (20.4 ± 1.2 µM). The result showed that ZnO (277.3 ± 15.6 µM) has the higher concentration of ROS generated than other metal oxides, which could be beneficial for inactivation of the growth of bacteria.

(ii) Interaction of cell membrane wall

A simple bacterium is made up of cytoplasm, cell membrane and cell wall. The cell wall lies outside the cell membrane. The functions of the cell wall are to provide the cell shape, rigidity, and avoid the cell from osmotic rupture and mechanical damage (Fu et al, 2005). Generally, bacteria can be categorized into two